Multi-dimensional chaos initiated by short pulses in non-autonomous radio-physical generator

Kilina A.[1,2], *Panteleeva P.*[1,2], *Stankevich N.*[1,2]*

[1]HSE University, 25/12 Bolshaya Pecherskaya Str., 603155 Nizhny Novgorod, Russia
[2]Leonhard Euler International Mathematical Institute, Saint Petersburg University, 7-9 Universitetskaya Embankment, 199034 St. Petersburg, Russia
* corresponding author: stankevichnv@mail.ru

Abstract. A non-autonomous model of the Anishchenko-Astakhov generator in the regime of periodic and chaotic self-oscillations is considered. A periodic sequence of short pulses is considered as an external force. It is shown that the synchronization picture is close in structure to the classical synchronization picture observed in a two-dimensional system, but the pulse action leads to the excitation of chaotic oscillations, including those characterized by a different spectrum of Lyapunov exponents. In particular, it is shown appearance of hyperchaos and chaos with additional close to zero Lyapunov exponent. Phenomenological scenarios for the development of multi-dimensional chaos related to destruction of two-frequency tori are described. Hyperchaos is formed via hierarchy of discrete Shilnikov attractors arise as a result of sequence of Neimark-Sacker bifurcations. Chaos with additional close to zero Lyapunov exponent occurs as impact of saddle tori appeared via sequence of torus-doubling bifurcations.

Keywords: non-autonomous system; pulsed action; multi-dimensional chaos; Lyapunov exponents; synchronization tongue; Neimark-Sacker bifurcation

1. Introduction

Synchronization of self-oscillatory systems is a classical problem of oscillation and wave theory, which is reflected in various fields of science and applications [1-3]. When an external signal is applied to a self-oscillatory system, the classical phenomenon of synchronization is observed. In this case, there is a set of synchronization tongues on the parameter plane of the external force: amplitude - period. These synchronization tongues correspond to the rational ratio of the own frequency of self-oscillations to the frequency of external force. The simplest case for such a situation is a two-dimensional self-oscillatory system on which an external signal is applied. In this case the non-autonomous system has a three-dimensional phase space, and more complex oscillatory regimes, such as chaotic can develop [4]. In the case when the autonomous system has dimension more than two, its autonomous dynamics can be more various, including quasi-periodic and chaotic oscillations. In the case of applying an external signal to chaotic oscillations, we can talk about the well-known phenomenon of synchronization through suppression of its own chaotic dynamics, and also about chaotic synchronization [5-6]. Also, the action can initiate various new effects for systems with dimension 3 or more, including excitation of multi-dimensional chaos. In works [7-9] it was shown that for three-dimensional systems the synchronization picture depends on the direction of action of the external signal on the example of the Rössler system under periodic force. The possibility of torus appearance and their bifurcation was also shown.

A specific case of interest is when the external force has the character of short in duration but significant in amplitude pulses. This type of external force is widespread in various fields of science, including applied ones. Big interest for this kind perturbation can be found in biology and medicine, since different manipulations (for example, injection), or taking pills changes state of object almost impulsively. One of the important problems it is vaccination which can be considered from different point of view and for different diseases [10-14]. Other medicine problems were considered in [15-16], which relate to pulsed external force. With pulses it is

possible to simulate a fast interacting systems, like neurons, lasers [17-19]. One also can meet pulsed forces in different engineering problems [20-22]. In some cases such type of external force can stabilize trajectories going to divergence [23].

In this work, we consider the features of a three-dimensional non-autonomous system with a single equilibrium point using as an example model of the Anishchenko-Astakhov generator, illustrate the possibility of the emergence of chaotic behavior, including multi-dimensional chaos in the case of periodic autonomous oscillations in the system, and in the case of chaos. We focuses on the example which is enough simple (it has single equilibrium point, and can be implemented as a self-oscillatory generator), but can demonstrate development of chaos. The novelty of the work is analysis of different types of chaotic behavior and description of scenarios for them formation. The obtained results can be applied for engineering problems: the pulsed action can control behavior of the system [23-25].

The work is structured as follows. In Section 2, as a review we present the result of the study of the van der Pol oscillator under periodic impulse force as a classical synchronization picture of a self-oscillatory system by a periodic sequence of short pulses. In Section 3, we present the main object of study: model of the Anishchenko-Astakhov generator; briefly describe the dynamics of the autonomous system and illustrate the dynamics of the model for selected operating parameters. In Section 4, we describe the synchronization picture for the Anishchenko-Astakhov generator under periodic pulse action in the self-oscillation mode, discuss the possibility of the development of multi-dimensional chaos and explain the phenomenological and bifurcation scenarios of its development. In Section 5, we present the results of modeling the Anishchenko-Astakhov system in chaos mode with periodic impulse force. Section 6 provides the main conclusions.

2. Classic synchronization picture with a periodic pulse signal on the example of van der Pol oscillator

One of the classical self-oscillatory systems is the van der Pol oscillator [26, 27]. The mathematical model of the van der Pol oscillator has the following form:

$$\ddot{x} - (\lambda - x^2)\dot{x} + \omega_0^2 x = 0. \tag{1}$$

Here λ is a parameter responsible for the excitation of self-oscillations in system (1), ω_0 is a parameter that determines the own frequency of self-oscillations of the oscillator (1). A supercritical Andronov-Hopf bifurcation occurs at $\lambda=0$, as a result of which a stable equilibrium point becomes an unstable focus and a stable limit cycle is born. Figure 1a shows an example of a limit cycle for $\lambda=1$, $\omega_0=1$.

Let us apply an external impulse force to the oscillator and rewrite a system in form of the first order ordinary differential equations:

$$\begin{aligned} \dot{x} &= y, \\ \dot{y} &= (\lambda - x^2)y - \omega_0^2 x + A\sum_{n=1}^{\infty}\delta(t - nT), \end{aligned} \tag{2}$$

where A is the amplitude, T is the period of the external force, n is the pulse number.

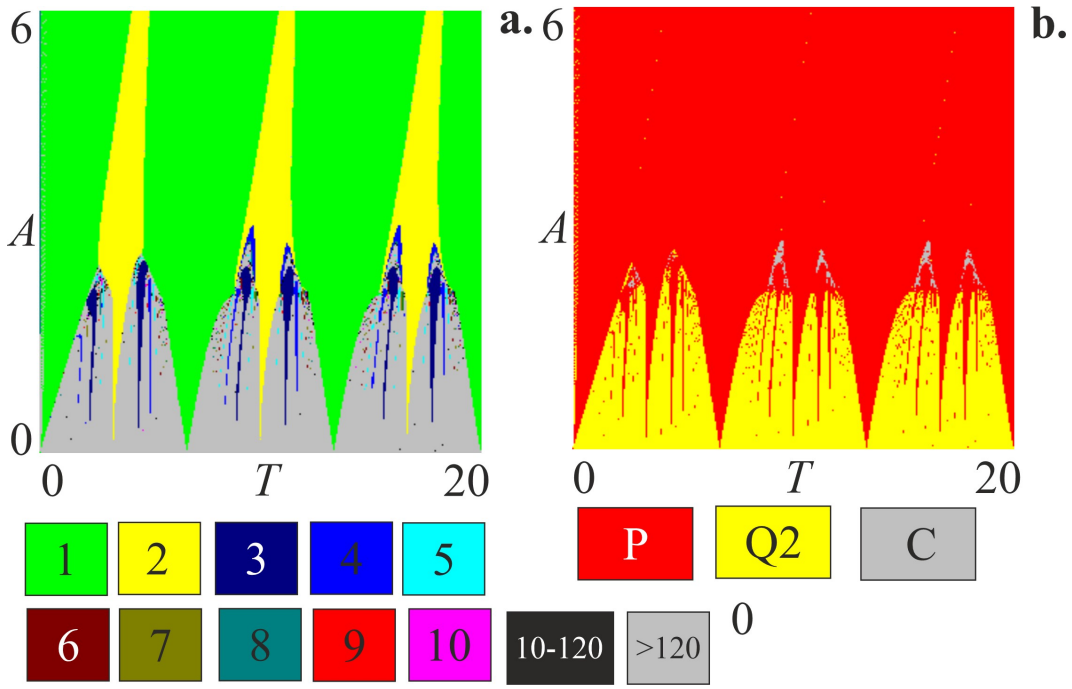

Fig.1. Synchronization picture of non-autonomous van der Pol oscillator excited by sequence of periodic pulses (2). a. Chart of dynamical regimes; **b.** Chart of Lyapunov exponents. Parameters: $\lambda=1$, $\omega_0=2\pi$. P is periodic oscillations; Q2 is two-frequency quasi-periodic oscillations; C is chaotic oscillations

Figures 1a and 1b show a chart of dynamical regimes and chart of Lyapunov exponents of model (2). The chart of dynamical regimes was constructed as follows: the parameter plane was scanned with a small step. For each point of the parameter plane, the regime was determined by the number of fixed points in the stroboscopic section[1]. Parameter plane points corresponding to periodic regimes were colored in different colors (the palette at the bottom of the chart is used for all chart of dynamical regimes). If the number of points in the stroboscopic section was more than 120, then we conclude that the observed regime is non-periodic and such point is colored in gray. Initial conditions were chosen fixed for $A=0$ as $x_0=0.5$, $y_0=0.51$. With increasing amplitude for the next value we use initial conditions from previous value of parameter A, in corresponding with [28]. Such technique can help to detect multistability in the system. The chart of Lyapunov exponents was constructed in a similar way, but when choosing the color of a point on the parameter plane, the full spectrum of Lyapunov exponents was analyzed. Lyapunov exponents were calculated according to the algorithm proposed in [29] with the Gram-Schmidt orthogonalization. Note, that in our numerical experiments, we determined so-called "finite-time local Lyapunov exponents" [30, 31]. Note that the spectrum of Lyapunov exponents was calculated for map in the stroboscopic section; therefore, one of the exponents, responded for the external force, always equal to zero, and it was not taken into account in the analysis. Classification of observed regimes was carried out in accordance with the following rule:

- periodic oscillations, P, $(0> \Lambda_1> \Lambda_2)$;
- two-frequency quasi-periodic oscillations, Q2, $(\Lambda_1=0, 0> \Lambda_2)$;
- chaotic, C, $(\Lambda_1>0, 0> \Lambda_2)$.

On the charts we clearly see the classic synchronization picture of a self-oscillatory system by external force. When the signal amplitude is small, two-frequency quasi-periodic oscillations arise, into which a system of synchronization tongues is built. In this system, one can distinguish the main tongues (period-1), which have their bases at points where the frequency (period) of self-oscillation coincides with the frequency (period) of external force. Tongues on subharmonics are also clearly visible when the frequencies ratio corresponds to some rational number. On the chart of Lyapunov exponents one can detect small areas of chaotic behavior that

[1] For solving all ordinary differential equations in the work we use 4^{th} degree Runge-Kutta methods with step integration less then 10^{-2}.

arise when synchronization tongues overlap. Areas of chaos are localized in the parameter space and at large values of the amplitude of the external signal, complex dynamics do not develop and periodic self-oscillations are observed. In works [4, 32-33] you can find a detailed description of the synchronization picture of a van der Pol oscillator excited by a pulse signal.

3. Objects and methods of research: autonomous and non-autonomous model of the Anishchenko-Astakhov generator

The main object of our study is a self-oscillatory system with a three-dimensional phase space - the model of Anishchenko-Astakhov generator [34], which is described by a system of three ordinary differential equations in the following form:

$$\begin{aligned} \dot{x} &= mx + y - xz, \\ \dot{y} &= -x, \\ \dot{z} &= -gz + g\Phi(x)x^2, \end{aligned} \tag{3}$$

where the function $\Phi(x)$ is a piecewise linear function defined as follows: $\Phi(x) = 0$, for $x \leq 0$ and $\Phi(x) = 1$, for $x > 0$. This model can be represented as a harmonic oscillator with an additional variable that modulates dissipation in the system:

$$\begin{aligned} \ddot{x} - (m - z)\dot{x} + x + x\dot{z} &= 0, \\ \dot{z} &= -gz + g\Phi(x)x^2. \end{aligned} \tag{4}$$

In this notation, it is clearly seen that the parameter m is responsible for dissipation in model (2), and the parameter g is responsible for the nonlinear feedback circuit. In model (3) there is a single trivial equilibrium point for which expressions for the eigenvalues can be obtained:

$$\lambda_1 = -g,\ \lambda_{2,3} = \frac{m \pm \sqrt{m^2 - 4}}{2} \tag{5}$$

Assuming the parameters are positive: m, $g > 0$, we can conclude that the only equilibrium point is a saddle-focus with a two-dimensional unstable manifold. In this case, the parameter g is responsible for compression along a one-dimensional stable manifold, and the parameter m is responsible for the unwinding of trajectories in a two-dimensional subspace. For $m > 2$, the saddle-focus equilibrium state is transformed into a saddle-node, while the dimensions of the stable and unstable manifolds remain the same. When $m = 0$ in model (3), an Andronov-Hopf bifurcation occurs, as a result of which a stable limit cycle is born. Figure 2 shows the bifurcation diagram (Fig. 2a), obtained using the numerical bifurcation analysis package XPPAUT [35], and the bifurcation tree (Fig. 2b). The diagram shows the dependence of the x-coordinate of equilibrium point and the maximum amplitude of the cycle on the variable m, and the colors also indicate the stability and types of equilibrium point and cycles (in the caption to Fig.2 a decoding is given). The bifurcation tree demonstrates the same dependence, but for attractor points in the Poincaré map with a cross-section plane $x = 0$. Figure 2b also shows plots of the two largest Lyapunov exponents (red and green color, the scale for Lyapunov exponents is depicted on the right of the Fig.2b). So, we can observe the development of chaos in the system. The bifurcation tree and Lyapunov exponents clearly shows the classical cascade of period-doubling bifurcations, which leads to the appearance of a chaotic attractor near a saddle-focus equilibrium point with a two-dimensional unstable manifold.

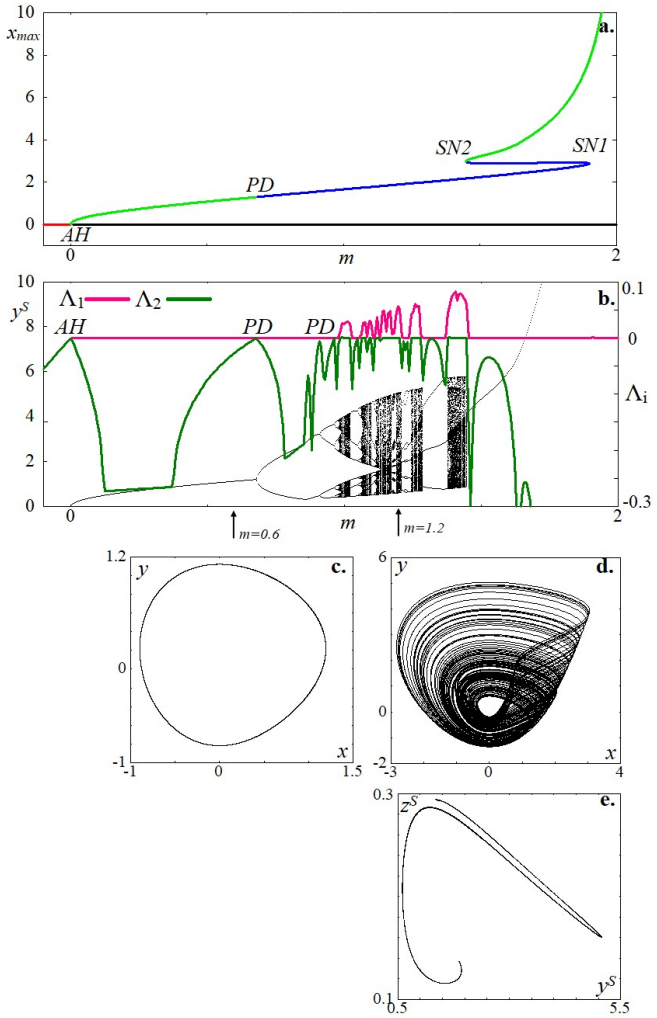

Fig.2. Dynamics of autonomous model of the Anishchenko-Astakhov generator (3). Parameters: g=0.5. **a.** bifurcation diagram (red/black color is a stable/ an saddle equilibrium point; green/blue is a stable/saddle limit cycle); **b.** bifurcation tree (black points, y^S) and plots of the two largest Lyapunov exponents (red and green lines, Λ_1, Λ_2); **c.-d.** phase portraits: **c.** m=0.6; **d.** m=1.2; **e.** map in the Poincaré section by the plane x=0, m=1.2. *AH* is Andronov-Hopf bifurcation; *PD* is period-doubling bifurcation; *SN* is saddle-node bifurcation

We choose two points, which are marked with arrows in Fig.2b, as operating parameters to study the dynamics of a non-autonomous system. For m=0.6 model (3) demonstrates stable periodic self-oscillations; Fig.2c shows this attractor. The oscillation period for the selected parameter is $T \approx 6.15$. The second value of the parameters corresponds to the chaotic behavior of the model at m=1.2, the corresponding attractor and his stroboscopic section presented in Fig.2d and 2e.

Let us move on to the description of the non-autonomous model. The model of the Anishchenko-Astakhov generator under periodic pulse action can be written as follows:

$$\begin{aligned} \dot{x} &= mx + y - xz, \\ \dot{y} &= -x + A\sum_{n=1}^{\infty}\delta(t - nT), \\ \dot{z} &= -gz + g\Phi(x)x^2. \end{aligned} \tag{6}$$

As well as for the van der Pol oscillator (2), here A, T are the amplitude and period of the external signal, n is the number of the pulse in the sequence. We added the external force to the second equation, since the y-variable represents the coordinate, in accordance with (4) and the analogy with the van der Pol oscillator.

We also use the chart of dynamical regimes and the Lyapunov exponent chart methods as the main research tool. The spectrum of Lyapunov exponents makes it possible to distinguish regions with quasi-periodic and chaotic dynamics for a four-dimensional model, as well as to

classify different types of chaos. The non-autonomous model (6) has a four-dimensional phase space; therefore, the full spectrum of Lyapunov exponents of such a system has 4 exponents. We also calculate Lyapunov exponents for stroboscopic section, which gives three significant Lyapunov exponents, excluding zero from the spectrum. Then in model (6), depending on the values of the Lyapunov exponents, the following types of dynamic behavior can be classified:

- periodic oscillations, P, ($0> \Lambda_1> \Lambda_2> \Lambda_3$);
- two-frequency quasi-periodic oscillations, Q2, ($\Lambda_1=0, 0> \Lambda_2> \Lambda_3$);
- three-frequency quasi-periodic oscillations, Q3, ($\Lambda_1= \Lambda_2=0, 0> \Lambda_3$);
- chaotic, C, ($\Lambda_1>0, 0> \Lambda_2> \Lambda_3$);
- hyperchaotic, HC, ($\Lambda_1> \Lambda_2>0, 0> \Lambda_3$).
- chaotic with additional zero (close to zero) Lyapunov exponent, C0, ($\Lambda_1>0, \Lambda_2=0, 0> \Lambda_3$).

Let us move on to studying the behavior of model (6).

4. Pulses action on the model of Anishchenko-Astakhov generator in the regime of periodic self-oscillations

4.1. Synchronization picture: main dynamical regimes, structure of parameter plane

First, we consider the picture of dynamical regimes when external force applied to a model with periodic self-oscillations. Figure 3 shows a chart of dynamical regimes and a chart of Lyapunov exponents at g=0.5, m=0.6. We used the parameters of the external signal as control parameters: period, T and amplitude, A. The starting initial conditions were fixed as x_0=0.5, y_0=0.51, z_0=0.52 for A=0, with increasing amplitude for the next value we use initial conditions from previous value of parameter A. The synchronization picture is close to that for the classical van der Pol oscillator (Fig. 1). Synchronization tongues of period-1 are observed at small amplitudes of external force. The bases of these tongues leave the points where the period of the external signal is a multiple to the period of self-oscillations of the model (3). The exit from the synchronization tongue corresponds to the saddle-node bifurcation and the change of the dynamical regime to two-frequency quasi-periodic oscillations. It is possible to detect tongues of regular oscillations with different periods within quasi-periodic oscillations. These are the so-called synchronization tongues at subharmonic frequencies. The tongues widen and overlapping with increasing amplitude of the external force and the torus collapse with the formation of chaotic oscillations is observed. In this case regions of complex behavior are localized in the parameter space. Stabilization of periodic self-oscillations occurs at a sufficiently large signal amplitude. It is precisely these characteristic features that can be observed in the non-autonomous van der Pol oscillator.

Let us study in more detail the areas of complex behavior. The charts clearly show that chaotic oscillations in the parameter plane occupy small regions, while they have two thresholds for the amplitude of the external signal: quasi-periodicity is observed below the overlap line of synchronization tongues. The upper threshold for the occurrence of chaos corresponds to various scenarios for its development as the signal amplitude decreases, which we consider further in Section 4.2. In this case, the dimension of the phase space of model (6) is greater than that of the van der Pol oscillator, which creates the possibility for the development of multi-dimensional chaos in a non-autonomous system. On the chart we can see to the left of the synchronization tongue at the base frequency a small area of hyperchaos (marked by a rectangle in Fig. 3b). Note that multidimensional chaos is destroyed with increasing period of the external signal, and we see only chaos with one positive and one zero Lyapunov exponent in the vicinity of doubled and tripled frequencies. We consider the features of the multi-dimensional chaos formation in Section 4.3.

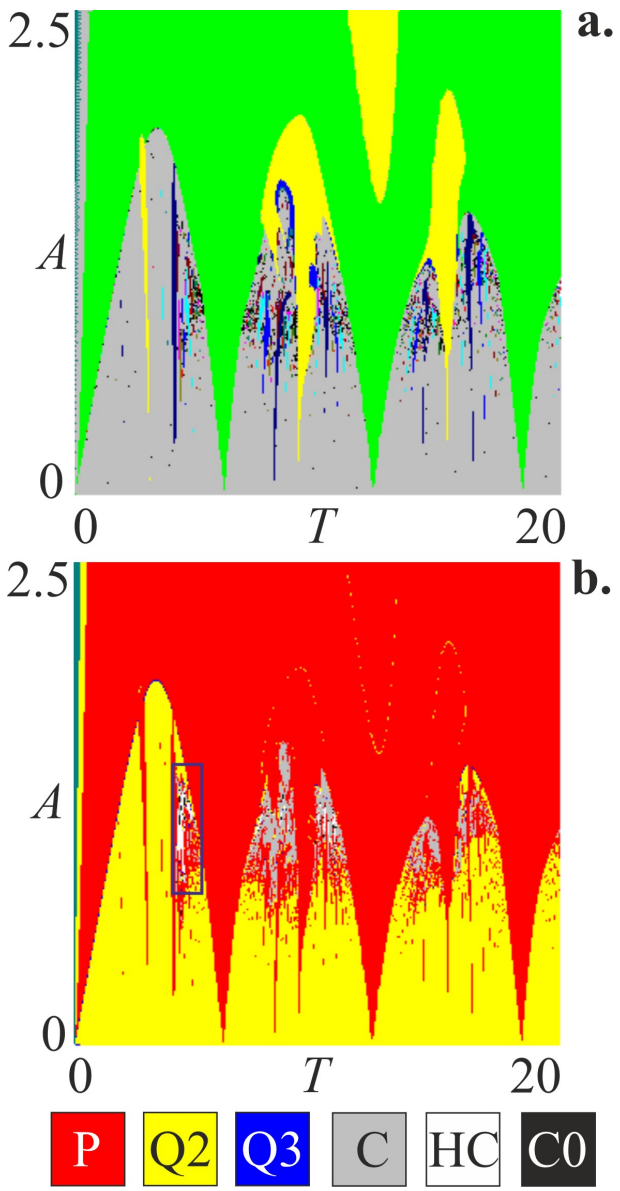

Fig.3. Synchronization picture of non-autonomous model of Anishchenko-Astakhov generator (6) in the regime of periodic self-oscillations. a. Chart of dynamical regimes; **b.** Chart of Lyapunov exponents. Parameters: g=0.5, m=0.6. P is periodic oscillations; Q2 is two-frequency quasi-periodic oscillations; Q3 is three-frequency quasi-periodic oscillations; C is classical chaos; HC is hyperchaos; C0 is chaos with additional zero (or close to zero) Lyapunov exponent

4.2. Upper threshold for the occurrence of chaos with amplitude decreasing

On the chart of dynamical regimes, as the signal amplitude decreases, three types of bifurcations that occur with the limit cycle can be observed: (i) period-doubling bifurcation; (ii) saddle-node bifurcation; (iii) Neimark-Sacker bifurcation. Saddle-node bifurcation occurs when leaving the synchronization tongue; as a result a pair of cycles merges and the dynamical mode is transformed into quasi-periodic, or chaotic. At the same time, chaos was formed as a result of some other scenario, which is associated with the period-doubling bifurcation or the Neimark-Sacker bifurcation.

Areas of chaos are formed before the appearance of periodic oscillations. This feature is due to the fact that in these areas the synchronization tongues at subharmonics overlap and merge. The period-doubling bifurcation lines are well traced on the chart, through which you can put a route on the parameter plane to the period-2 synchronization tongue. A decrease in amplitude within each tongue leads to the development of chaos either through a cascade of period-doubling bifurcations or through a Neimark-Sacker bifurcation. Figure 4 shows an enlarged fragment of the chart of Lyapunov exponents in the vicinity of the synchronization

tongue at $T \approx 3T_0$. To the left of the period-2 tongue, a cascade of period-doubling bifurcations and the development of chaos can be clearly seen. However, this chaos is not multi-dimensional.

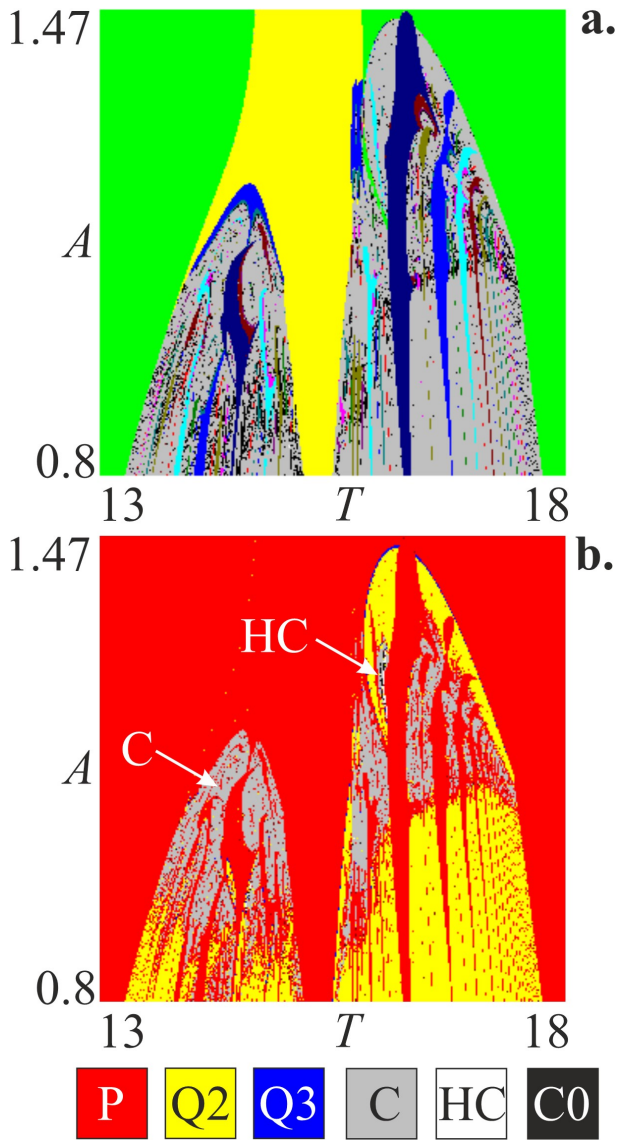

Fig.4. Structure of parameter plane near area of chaos formation of non-autonomous model of Anishchenko-Astakhov generator (6). a. Chart of dynamical regimes; **b.** Chart of Lyapunov exponents. Parameters: g=0.5, m=0.6. P is periodic oscillations; Q2 is two-frequency quasi-periodic oscillations; Q3 is three-frequency quasi-periodic oscillations; C is classical chaos; HC is hyperchaos; C0 is chaos with additional zero (or close to zero) Lyapunov exponent

A Neimark-Sacker bifurcation line based on the period-1 cycle locates to the right from the period-2 synchronization tongue, a family of synchronization tongues of different periods is observed along the bifurcation line, the overlap of tongues can lead to the development of hyperchaos, in Fig. 4b this area is marked with the symbol HC. Thus, multi-dimensional chaos is also observed for large values of the period of external force, but the areas with such dynamics are very small in the parameter plane.

4.3. Multi-dimensional chaos formation

Let us consider the features of the multi-dimensional chaos formation in model (6). Multi-dimensional chaos is formed as a result of the destruction of a two-frequency torus. As mentioned earlier, by multi-dimensional chaos we mean chaotic attractors, which are characterized either by several positive Lyapunov exponents, or the spectrum has additional zero (or close to zero) exponent. Both types of such multi-dimensional chaos can arise as a result of the destruction of a two-dimensional invariant torus. In the case of a four-dimensional flow

model, there can be only two types of multi-dimensional chaos in dependence on Lyapunov exponents spectrum signature: (i) hyperchaos (+, +, 0, -); (ii) chaos with an additional zero Lyapunov exponent (+, 0, 0, -). In recent works [36-42] new scenarios for the development of these kinds of attractors through the destruction of a two-dimensional invariant torus were shown.

The key point for the formation of chaotic attractors of various types is the accumulation of the set of cycles that forms the skeleton of a chaotic attractor. Thus, the skeleton of a classical chaotic attractor consists of saddle cycles with a one-dimensional unstable manifold. These are cycles with a two-dimensional unstable manifold for hyperchaos. For a four-dimensional system, we can assume two types of bifurcations that give such cycles: (i) Neimark-Sacker bifurcation of a stable cycle; (ii) period-doubling bifurcation of a saddle cycle with a one-dimensional unstable manifold.

The situation is more complex for chaos with an additional zero Lyapunov exponent. One of the possibilities for creating trajectories characterized by such a spectrum of Lyapunov exponents is the formation of a set of saddle tori with a one-dimensional unstable and two-dimensional neutral manifold. The torus doubling bifurcation may lead to the appearance of such torus. A smooth invariant torus loses stability as a result of period-doubling bifurcation, torus becomes a saddle. It has a one-dimensional unstable manifold, while a two-dimensional neutral manifold can be preserved and a stable ergodic torus of double period is born in its neighborhood. A cascade of tori-doubling bifurcations forms a set of saddle tori. As a result of the absorption of saddle tori by a chaotic attractor and provided that they are preserved, additional zero Lyapunov exponents (or close to zero) may appear in the spectrum of exponents of such an attractor, the number of which depends on the dimension of the torus [42]. Such attractors were first shown on examples of maps and non-autonomous systems in [43-44] and were called quasi-periodic Hénon-like attractors. They represent the product of the Hénon attractor and the torus. Another possibility for the formation of saddle tori is the loss of smoothness of a three-dimensional ergodic torus [41]. Recent work has described a similar scenario for coupled flow systems [41-42] and also in other applications [45].

Let us consider the features of the formation of multidimensional chaos in our model. A small area of hyperchaos appeared as a result of the destruction of the torus identifies in Fig.4b. The area of multi-dimensional chaos for small values of period of external force is most pronounced in Fig. 3b to the left of the period-3 synchronization tongue (in Fig. 3b this area is marked with a rectangle). Figure 5a shows a zoomed fragment of the chart of Lyapunov exponents. The chart clearly identifies the Neimark-Sacker bifurcation line (l_{NS}), the period-doubling bifurcation lines (l_{PD}), and the saddle-node bifurcation line (l_{SN}). Along the Neimark-Sacker bifurcation line, a system of synchronization tomgue embedded in the region of two-frequency quasi-periodicity is visible. Within the tongue, it is possible to trace cascades of period-doubling bifurcations of stable cycles and the development of classical chaos, which then develops into hyperchaos. There are also secondary Neimark-Sacker bifurcations within synchronization tongues, which lead to the development of a hierarchy of hyperchaotic attractors [39]. On the chart it is possible to trace the bifurcation line of invariant torus doubling. This line can be identified using the rigorous analysis of Lyapunov exponents proposed in [46-47]. Before and after bifurcation threshold, a stable two-dimensional torus is observed in the system, which is characterized by two zero Lyapunov exponents, the third exponent also becomes zero at the moment of bifurcation. Thus, thin blue lines[2] in the region of two-dimensional tori correspond to tori doubling bifurcations (l_{TD}). So, there is an opportunity for the development of chaos with an additional zero Lyapunov exponent in accordance with the scenario described above.

[2] Blue color corresponds to the equality of three the largest Lyapunov exponents to zero.

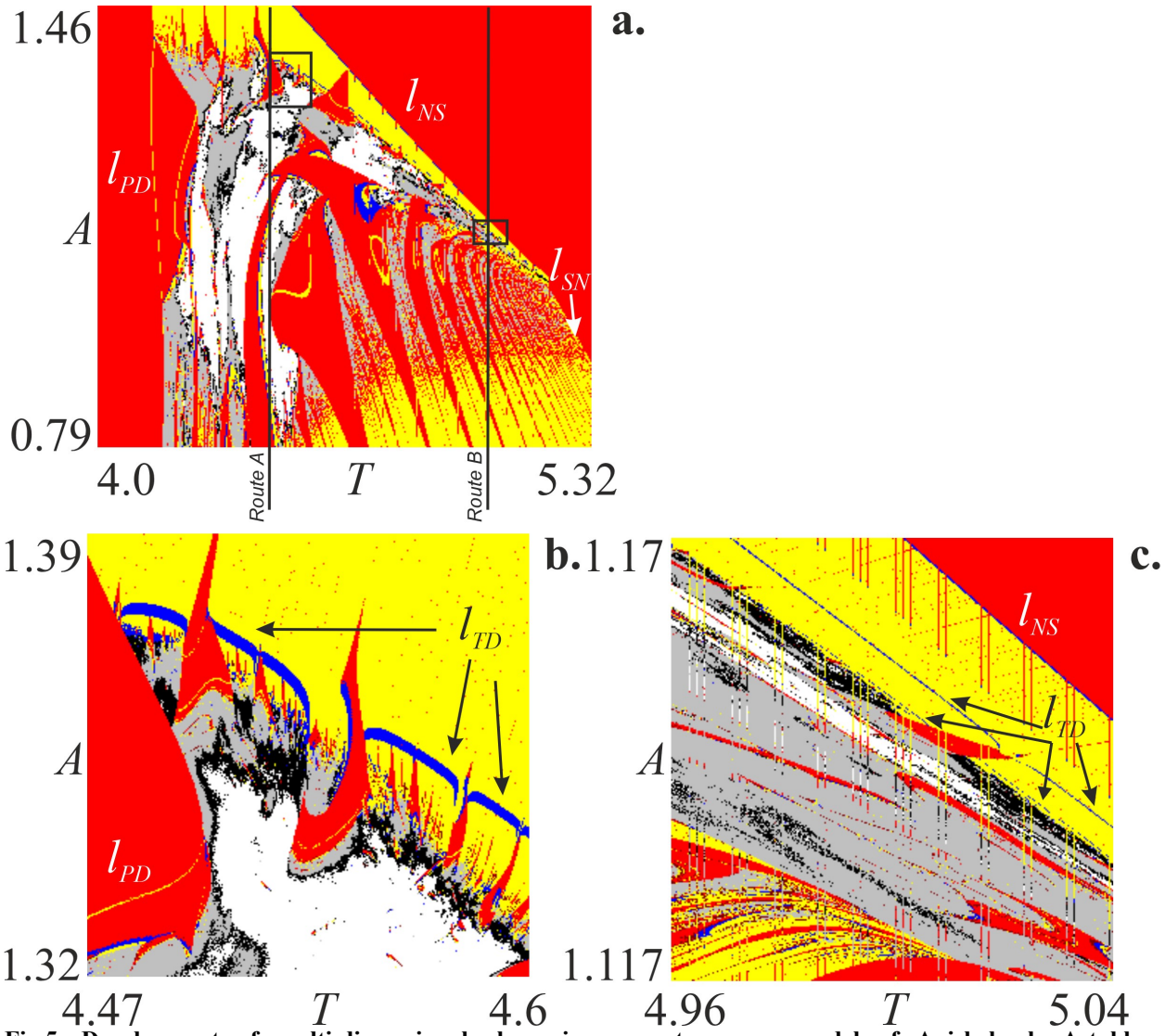

Fig.5. Development of multi-dimensional chaos in non-autonomous model of Anishchenko-Astakhov generator (6). a. – c. Zoomed fragments of chart of Lyapunov exponents. Parameters: g=0.5, m=0.6. l_{NS} is line of Neimark-Sacker bifurcation; l_{PD} is line of period-doubling bifurcation; l_{SN} is line of saddle-node bifurcation; l_{TD} is line of torus-doubling bifurcation

Figure 5b and 5c show fragments demonstrating details of the parameter plane structure. The fragment in Fig. 5b depicts the features of the hyperchaos formation. The fragment in Fig. 5c makes it possible to trace several torus doubling bifurcations and a region of chaos with an additional zero (or close to zero[3]) Lyapunov exponent.

Let us analyze the scenario for the development of chaos using graphs of Lyapunov exponents and maps obtained with the stroboscopic section. Figure 6 shows the corresponding illustrations for T=4.47 (*Route A* in Fig. 5a). *Route A* crosses an area of hyperchaos within a wide range of the parameter A. Chaotic behavior, including hyperchaos, is well identified on the graph of Lyapunov exponents (Fig. 6a); it is localized in a certain interval according to the parameter. Periodic and quasi-periodic oscillations are observed for larger and smaller values of the parameter A. The external force in a non-autonomous system excites two-frequency quasi-periodic oscillations, which we observe for small values of the amplitude of the external signal. The torus loses its smoothness at A≈0.625 and the oscillations become chaotic.

Figure 6b shows an enlarged fragment of the Lyapunov exponents graphs, where one can track the development of classical chaos through the loss of smoothness of the torus, which is accompanied by the appearance of synchronization tongues. Figures 6c and 6d show

[3] When constructing charts, we used the following threshold to determine zero: $|\Lambda_i|<3*10^{-3}$.

corresponding examples of an invariant curve and a chaotic attractor in a stroboscopic section for small amplitudes of external force.

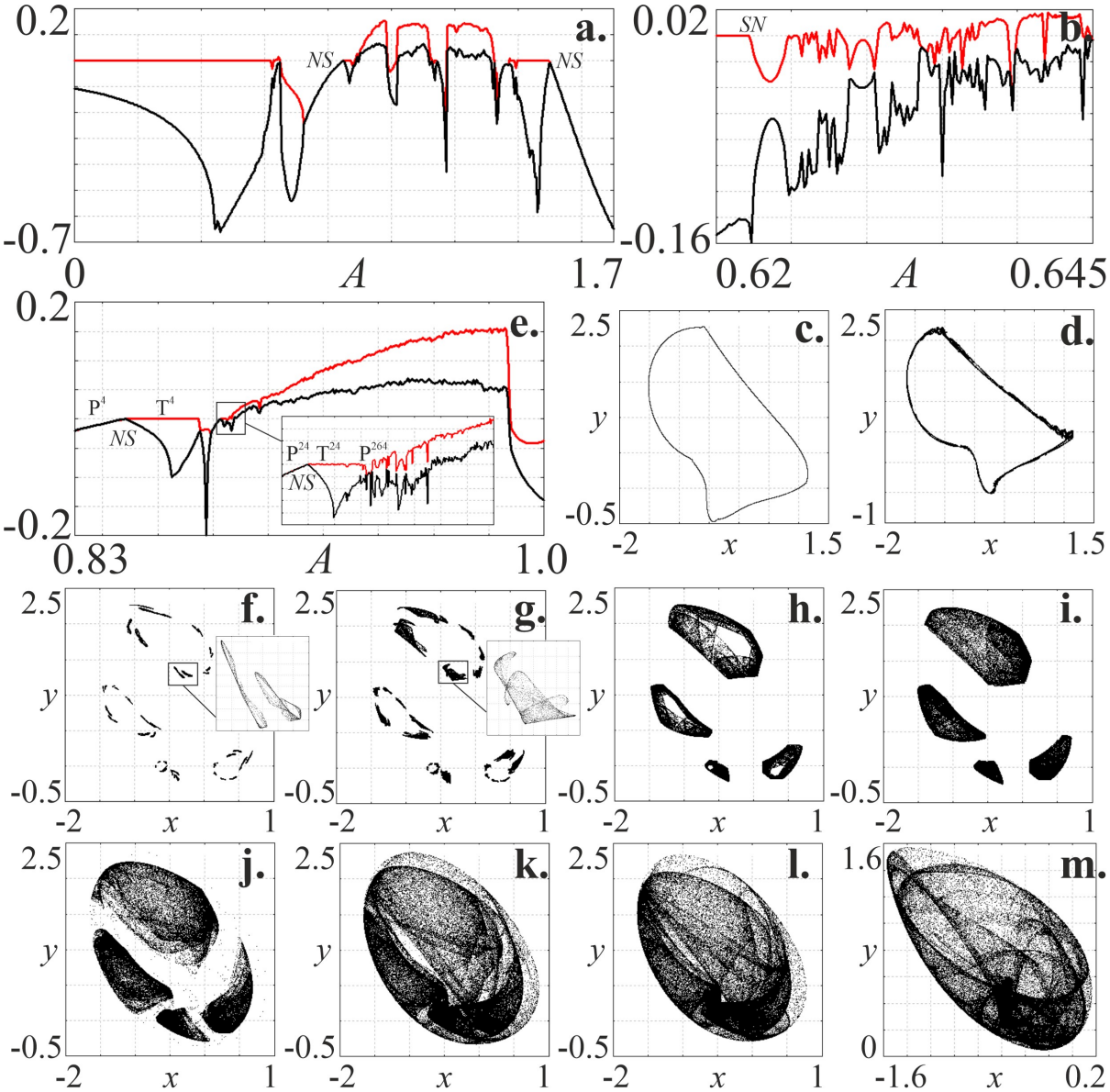

Fig.6. Development of hyperchaos in non-autonomous model of Anishchenko-Astakhov generator (6). Parameters: g=0.5, m=0.6, T=4.47 (*Route A* in Fig.5a). **a.**, **b.**, **e.** Graphs of the two largest Lyapunov exponents; **c.**, **d.**, **f.** – **m.** Maps in stroboscopic section: **c.** A=0.62; **d.** A=0.643; **f.** A=0.887; **g.** A=0.888; **h.** A=0.89; **i.** A=0.9; **j.** A=0.91; **k.** A=0.94; **l.** A=0.98; **m.** A=1.25. *NS* is Neimark-Sacker bifurcation; *SN* is saddle-node bifurcation

Hyperchaos develops with a further increase in the amplitude of external force A. Figure 6e shows a fragment of the graph of Lyapunov exponents at the threshold of the hyperchaos formation. The two-frequency torus becomes resonant at a certain value of the parameter A. A stable limit cycle of period-4 appears (P^4 in Fig. 6e). This cycle undergoes a Neimark-Sacker bifurcation and a stable invariant curve is born in the vicinity of each fixed point in the stroboscopic section. On the graph of Lyapunov exponents we see the emergence of two-frequency quasiperiodic oscillations (T^4 in Fig. 6e). A further increase in amplitude leads to a new resonance, which corresponds to a 6-fold resonance on a 4-component torus (P^{24} in Fig. 6e). There is a secondary Neimark-Sacker bifurcation with this cycle. This bifurcation is demonstrated in an enlarged fragment of the graph in Fig. 6e; the interval where a stable ergodic torus (T^{24}), which is represented by 24 invariant curves in the stroboscopic section, is clearly visible. Then resonance arises again, and 11 fixed points appear on each invariant curve in the stroboscopic section, which corresponds to a stable limit cycle of period 264 (4*6*11, P^{264}). The destruction of the torus occurs after this cycle and classical chaos arises. Figure 6f shows an

example of a classical chaotic attractor. This is a 48 component attractor. The enlarged fragment clearly shows that the attractor is distanced from the saddle-focus cycle of period 264. Then the regime is transformed into hyperchaos through homoclinic bifurcations of saddle-focus cycles with a two-dimensional unstable manifold. Figure 6g shows an example of an already hyperchaotic attractor. Hyperchaos is a 24-component attractor, it includes a saddle-focus cycle of period 264, and we also see in the enlarged fragment that each component of the attractor is filled with points inside, respectively, the attractor also includes a saddle-focus cycle of period 24. Table 1 shows the values Lyapunov exponents for the presented attractors, which confirm the emergence of hyperchaos. Figure 6h shows a 4-component hyperchaotic attractor, including a saddle-focus cycle of period 24. A homoclinic bifurcation occurs with a further increase in amplitude. The period 4 saddle-focus cycle is absorbed as a result of this bifurcation (Fig. 6i). Figure 6k depicts one-component hyperchaotic attractor that does not include a period-1 saddle-focus cycle: 4 components merge into one with a further increase in amplitude. Figure 6l shows an example of an attractor after the bifurcation of the emergence of a homoclinic orbit between a saddle-focus cycle of period-1 and a chaotic attractor. Figure 6m demonstrates an example of a similar hyperchaotic attractor, which occurs for large amplitudes of external force. Its development can also be tracked from a two-frequency torus with a decrease in signal amplitude.

Table 1. Values of the Lyapunov exponents for different chaotic attractors observed in non-autonomous model of Anishchenko-Astakhov generator (6) at the threshold of hyperchaos formation, $g = 0.5$, $m = 0.6$

T	A	Λ_1	Λ_2	Λ_3	Λ_4
4.47	0.643	0.0171	0.0	-0.0124	-1.6703
4.47	0.887	0.0071	0.0	-0.0078	-1.6432
4.47	0.888	0.0121	0.0011	0.0	-1.6571
4.47	0.89	0.0188	0.0075	0.0	-1.6723
4.47	0.9	0.0383	0.0267	0.0	-1.6913
4.47	0.91	0.0579	0.0325	0.0	-1.6621
4.47	0.94	0.1147	0.0567	0.0	-1.6273
4.47	0.98	0.1522	0.0518	0.0	-1.5840
4.47	1.25	0.1410	0.0242	0.0	-1.3913

Thus, the formation of a hierarchy of discrete chaotic Shilnikov attractors, which are hyperchaotic attractors, is shown. Note that the absorption of saddle-focus cycles with a two-dimensional unstable manifold of different periods is well reflected in the values of the Lyapunov exponents; the absorption of a new saddle cycle increases both of the largest positive Lyapunov exponents.

Now let us turn to the study of the formation of chaotic attractors with an additional zero Lyapunov exponent. The enlarged fragment in Fig. 5c shows areas with such dynamics. Note that the question of the accuracy of calculating Lyapunov exponents for this type of chaos is fundamentally important. In some situations, when not only saddle tori, but also saddle cycles with different dimensions of an unstable manifold contribute to the dynamics of the system, the additional zero Lyapunov exponent may not be zero, but close to zero. This situation is discussed in, for example [48-49].

We will also analyze a graphs of Lyapunov exponents and stroboscopic sections of phase portraits to study the mechanism of formation of such attractors. Figure 7 shows the corresponding illustrations for T=4.99 (*Route B* in Fig. 5a). Figure 7a shows a fragment of the graph where the emergence of chaotic behavior is observed. The area of complex dynamics is localized in the parameter space as in the previous case. There is a stable ergodic torus at small amplitudes, the loss of smoothness of which leads to the appearance of classical chaotic behavior. Self-oscillations of period-1 occur for large amplitudes. Corresponding limit cycle loses stability through the Neimark-Sacker (*NS*) bifurcation with decreasing amplitude and a torus is born. The ergodic torus undergoes two doubling bifurcations (*TD*) for a given choice of external force period. Figures 7d and 7e show examples of invariant curves in the stroboscopic section after the first and second bifurcation. After two bifurcations in the graph of Lyapunov exponents (Fig. 7c), we can see that periodicity windows appear and the invariant curve

collapses. At the same time, the graph clearly shows that the chaos that appears in the system has a second Lyapunov exponent close to zero.

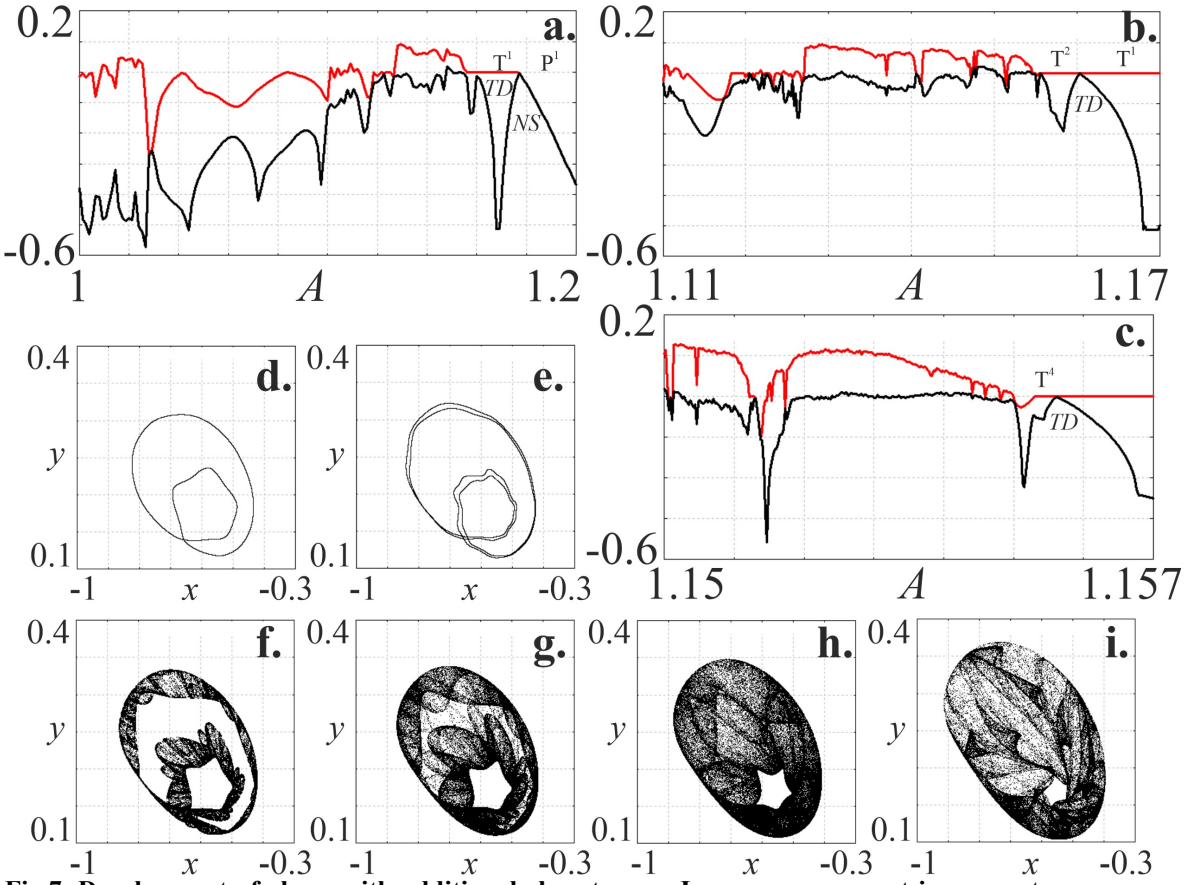

Fig.7. Development of chaos with additional close to zero Lyapunov exponent in non-autonomous model of Anishchenko-Astakhov generator (6). Parameters: g=0.5, m=0.6, T=4.99 (*Route B* in Fig.5a). **a.**, **b.**, **c.** Graphs of the two largest Lyapunov exponents; **d.** – **i.** Maps in stroboscopic section: **d.** A=1.157; **e.** A=1.1555; **f.** A=1.1545; **g.** A=1.154; **h.** A=1.153; **i.** A=1.151. *NS* is Neimark-Sacker bifurcation; *TD* is torus-doubling bifurcation

Figures 7f-7i show examples of stroboscopic maps for chaotic attractors with a second exponent close to zero. Table 2 presents the spectra of Lyapunov exponents, where one can see that the second exponent is close to zero, but is still weakly positive. The absence of a zero exponent in the spectrum is primarily due to the presence of resonances. Resonance cycles can be destroyed through Neimark-Sacker bifurcations which can lead to the appearance of saddle cycles with a two-dimensional unstable manifold in the attractor. The presence of saddle cycles is also possible, demonstrating cascades of period-doubling bifurcations. For smaller amplitude values, in the example of Fig. 7i, we can observe the transformation of the regime into classical chaos; we can see the concentration of points in the vicinity of some manifolds that correspond to saddle cycles with a one-dimensional unstable manifold. The uniformity of the distribution of points along the attractor is characteristic of attractors with an additional zero Lyapunov exponent [41-42].

Thus, we have shown that in the case of short pulses action to the model of the Anishchenko-Astakhov generator in the self-oscillation mode, hyperchaos can be excited, and chaos with an additional Lyapunov exponent close to zero occurs. Hyperchaos develops via secondary Neimark-Sacker bifircations, The occurrence of chaos with additional close to zero Lyapunov exponent is associated with the torus doubling bifurcation cascade.

Table 2. Values of the Lyapunov exponents for different chaotic attractors observed in non-autonomous model of Anishchenko-Astakhov generator (6) at the threshold of chaos with additional close to zero Lyapunov exponent formation, g = 0.5, m = 0.6

T	A	Λ_1	Λ_2	Λ_3	Λ_4
4.99	1.1545	0.0161	0.0	-0.0011	-1.0251

4.99	1.154	0.0312	0.0034	0.0	-1.0449
4.99	1.153	0.0525	0.0008	0.0	-1.624
4.99	1.151	0.0509	0.0	-0.0163	-1.0413

5. Pulses action on the model of Anishchenko-Astakhov generator in the regime of chaotic self-oscillations

5.1. Synchronization picture: main dynamical regimes, structure of parameter plane

Let us consider how regions of chaos are transformed in the parameter plane in the case of the development of chaotic dynamics in an autonomous system. In Sect. 3, we presented the parameters at which chaotic behavior is observed in system (3). Let us fix the parameters in this way and study non-autonomous system.

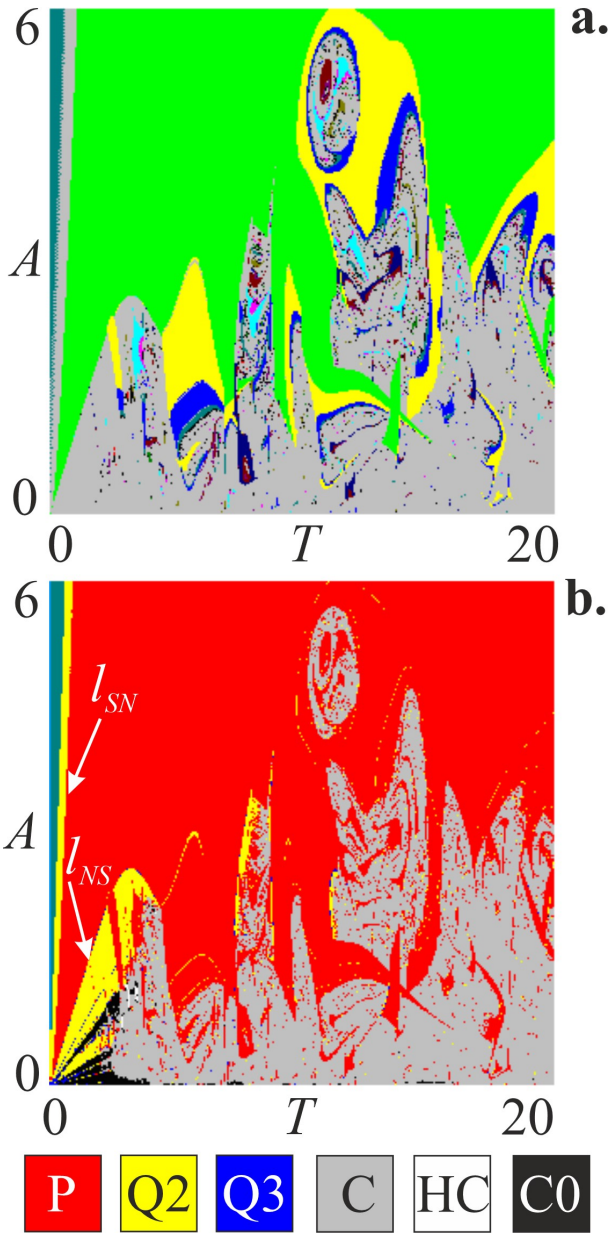

Fig.8. Synchronization picture of non-autonomous model of Anishchenko-Astakhov generator (6) in the regime of chaotic self-oscillations. a. Chart of dynamical regimes; **b.** Chart of Lyapunov exponents. Parameters: g=0.5, m=1.2. P is periodic oscillations; Q2 is two-frequency quasi-periodic oscillations; Q3 is three-frequency quasi-periodic oscillations; C is classical chaos; HC is hyperchaos; C0 is chaos with additional zero (or close to zero) Lyapunov exponent. l_{NS} is line of Neimark-Sacker bifurcation; l_{SN} is line of saddle-node bifurcation

Figure 8 shows charts of dynamical regimes and of Lyapunov exponents for the case of chaotic dynamics of autonomous model. It is clearly seen that the picture of the regimes has changed greatly in comparison with what it was for periodic self-oscillations. The family of synchronization tongues has collapsed and chaotic behavior is observed at low external force

amplitudes. Note that for signal amplitude values close to zero, chaos with an additional zero Lyapunov exponent is identified on the chart. It transforms into classical chaos with increasing amplitude of the external signal. We see suppression of the intrinsic dynamics for large values of the strength of external force parameter and stable oscillations of period-1 are realized in the system. With a decrease in amplitude, we can also observe two main scenarios for the development of chaos, which were also for the previous case: a cascade of period-doubling bifurcations and the destruction of the invariant torus, born as a result of the Neimark-Sacker bifurcation. The dominance of classical chaos, characterized by one positive and one zero Lyapunov exponent, is observed for large values of the period of external force. We also note that the Neimark-Sacker bifurcations are not detected in this region. Areas of two-frequency tori are observed at small values of the period of the external signal (high-frequency action). It is possible to trace the lines of torus-doubling bifurcations and the development of chaos with an additional zero Lyapunov exponent.

5.2. Multi-dimensional chaos formation

Let us consider in more detail the features of the emergence of multi-dimensional chaos. We constructed a zoomed fragment of the Lyapunov exponents chart for small values of the period of external force (Fig. 9a). The chart clearly shows areas of chaos with an additional zero Lyapunov exponent, as well as small areas of hyperchaos. The fragment depicts that several bifurcation lines emerge from the point of zero amplitude and period of the external force, forming a picture of the modes: there is a tongue of complete synchronization, the exit from which occurs through a saddle-node bifurcation with an increase in the amplitude of the external force (line l_{SN} in Fig.9a). The transition to quasi-periodic oscillations with decreasing amplitude occurs through the Neimark-Sacker bifurcation (line l_{NS} in Fig.9a), as a result of which a stable two-dimensional torus is softly born. The invariant torus undergoes a cascade of torus-doubling bifurcations (line l_{TD} in Fig.9a) with a further decrease in the amplitude of the external force. As a result of cascade chaos is formed with an additional Lyapunov exponent close to zero. This region is quite uniform for small values of the parameter T; tongues of two-frequency quasi-periodicity are observed inside it. The transformation of chaos with an additional zero into classical chaos is observed, as well as the formation of small areas of hyperchaos with an increase in the period of external force T.

Figures 9b, 9c show graphs of Lyapunov exponents for T=1.5 (*Route C* in Fig. 9a) to analyze the features of the emergence of chaos with an additional zero Lyapunov exponent. Three bifurcations of invariant torus doubling (*TD*) can be traced in the graphs. Figure 9d shows an example of an 8-turn invariant curve after the third doubling bifurcation. The torus loses smoothness with a further decrease in the signal amplitude A. Figure 9f shows an example of a weak chaotic attractor, the largest Lyapunov exponent is very small in value, but positive. Table 3 presents the values of Lyapunov exponents for the shown attractors, calculated with high accuracy. The merging of the torus components with a further decrease in amplitude is observed, which corresponds to the homoclinic bifurcation of the saddle tori and the chaotic attractor. Figure 9f shows an example of a chaotic attractor in a stroboscopic section, which has the structure of a 4-turn invariant curve. The third Lyapunov exponent of this attractor is close to zero (see Table 3). Figure 9g presents an example of a chaotic attractor after the next homoclinic bifurcation with a two-turn saddle torus. According to the spectrum of Lyapunov exponents, weak hyperchaos is diagnosed for this attractor, but the second positive exponent is also very close to zero, which indicates the contribution of the trajectory motion along the surface of the saddle tori. Figure 9h depicts the case where a single-turn torus was absorbed. In this case, there is no hyperchaos, the third negative Lyapunov exponent is very close to zero.

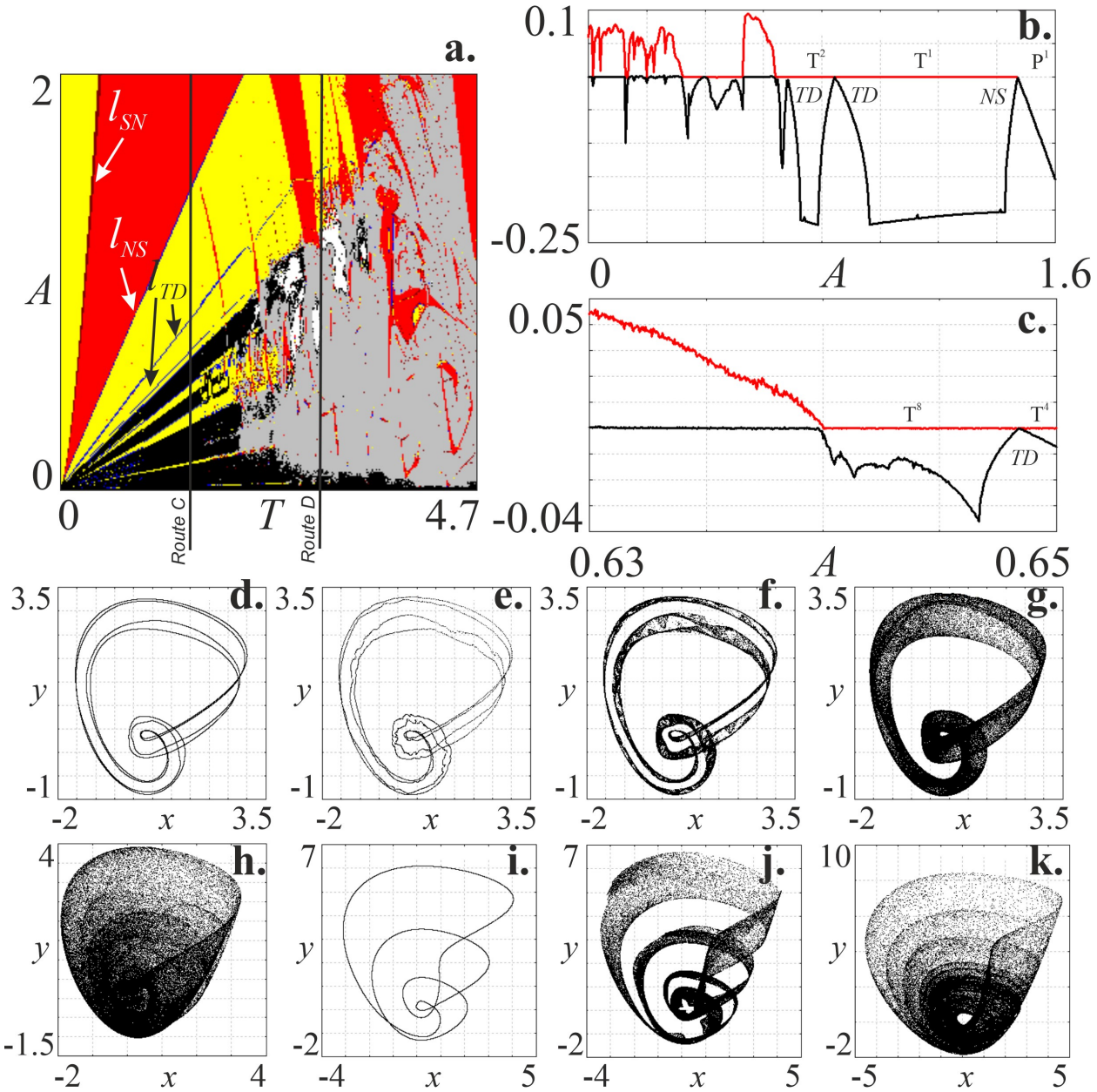

Fig.9. Development of chaos with additional close to zero Lyapunov exponent in non-autonomous model of Anishchenko-Astakhov generator (6). a. Chart of Lyapunov exponents. Parameters: g=0.5, m=1.2. **b.**, **c.** Graphs of the two largest Lyapunov exponents, T=1.5 (*Route C* in Fig.9a); **d.** – **k.** Maps in stroboscopic section: **d.** A=0.645; **e.** A=0.64; **f.** A=0.639; **g.** A=0.63; **h.** A=0.57; **i.** A=0.35; **j.** A=0.3; **k.** A=0.1. l_{NS}, *NS* are line and point of Neimark-Sacker bifurcation; l_{TD}, *TD* are line and point of torus-doubling bifurcation; l_{SN} is line of saddle-node bifurcation

Table 3. Values of the Lyapunov exponents for different chaotic attractors observed in non-autonomous model of Anishchenko-Astakhov generator (6) at the threshold formation of chaos with additional close to zero Lyapunov exponent, g = 0.5, m = 1.2

T	A	Λ_1	Λ_2	Λ_3	Λ_4
1.5	0.64	0.0002	0.0	-0.0029	-0.3961
1.5	0.639	0.0098	0.0	-0.0001	-0.4232
1.5	0.63	0.0453	0.0003	0.0	-0.4552
1.5	0.57	0.0878	0.0	-0.0001	-0.5249
1.5	0.3	0.0292	0.0004	0.0	-0.6137
1.5	0.1	0.0693	0.0	-0.0001	-0.6843

As noted above, within regions of chaos with an additional zero Lyapunov exponent, regions of two-frequency tori can be seen. Figure 9i shows an example of a map in a stroboscopic section, where it is clear that a multi-turn invariant curve occurs. This invariant curve can also collapse in accordance with the scenario described above, and in this case the invariant curve does not double. For the chaotic attractor in Fig. 9j, the spectrum of Lyapunov

exponents also contains additional Lyapunov exponent close to zero (see Table 3). Figure 9k presents an example of a chaotic attractor that includes saddle tori, both a basic one-turn invariant torus and a multi-turn torus, in the spectrum of Lyapunov exponents of which there is an additional Lyapunov exponent close to zero.

A fragment of the chart of Lyapunov exponents (Fig. 9a) clearly shows that for large values of the parameter T the emergence of hyperchaos can be observed. Let us consider scenarios for the occurrence of hyperchaos at T=3 (*Route D* in Fig. 9a); the corresponding illustrations are shown in Fig.10.

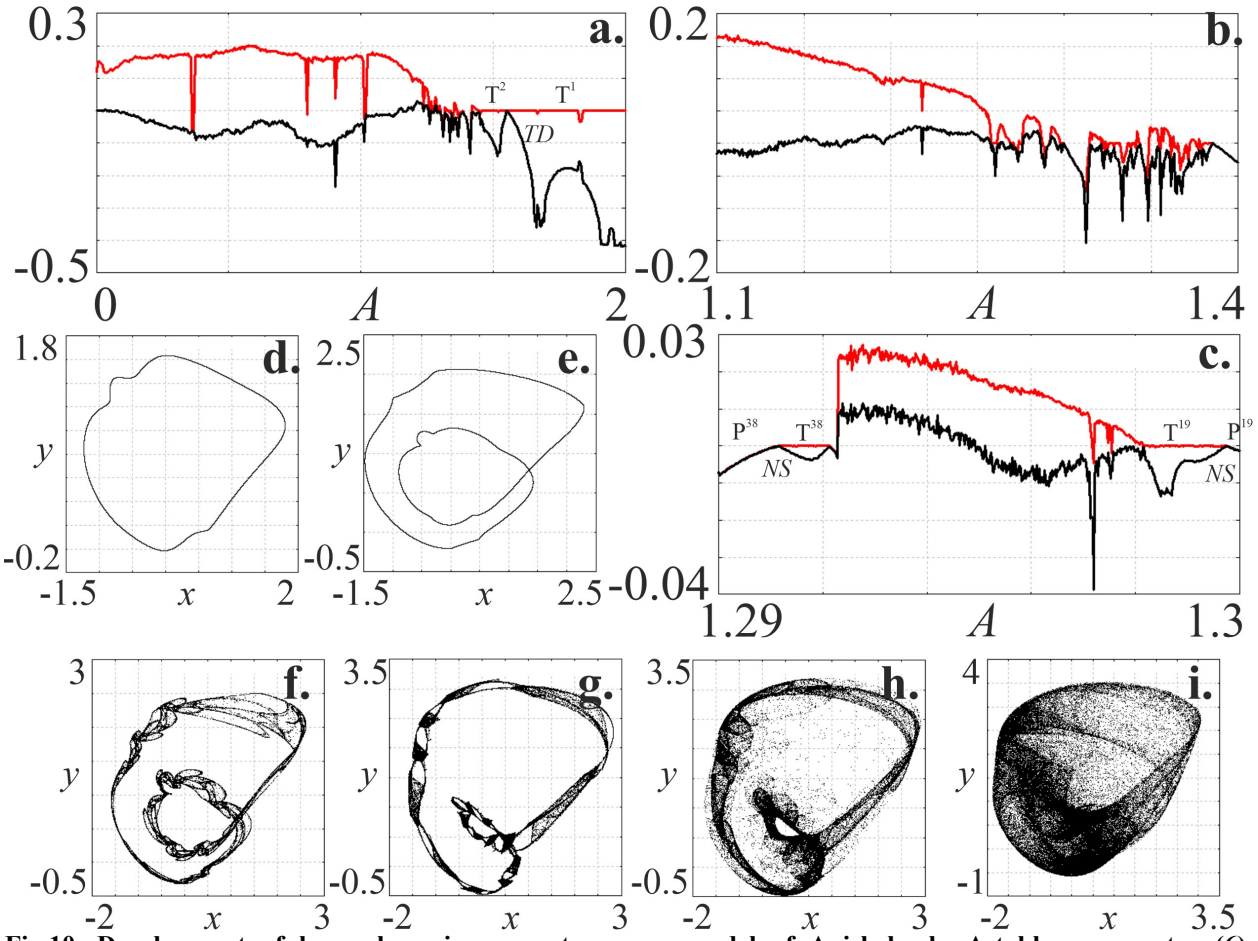

Fig.10. Development of hyperchaos in non-autonomous model of Anishchenko-Astakhov generator (6). Parameters: g=0.5, m=1.2, T=3.0 (*Route C* in Fig.9a). **a.**, **b.**, **c.** Graphs of the two largest Lyapunov exponents; **d.** – **i.** Maps in stroboscopic section: **d.** A=0.62; **e.** A=0.643; **f.** A=0.887; **g.** A=0.888; **h.** A=0.89; **i.** A=0.9. *NS* is Neimark-Sacker bifurcation; *TD* is torus-doubling bifurcation

At sufficiently large amplitudes of the external signal, two-frequency quasiperiodic oscillations are observed, as well as a torus doubling bifurcation. Figures 10d and 10e show the corresponding one-turn and double-turn invariant curves. The invariant curve has a complex shape; a further decrease in the amplitude A leads to the fact that the doubled invariant curve becomes resonant, loses smoothness, collapses and transforms into chaos (Fig. 10f). It is possible to diagnose small areas of hyperchaos on the graph of Lyapunov exponents in a wide range of changes in the amplitude parameter (Fig. 10a). Figure 10b and 10c show enlarged fragments in the area where hyperchaos occurs. Hyperchaos in this case is also formed through the absorption of saddle-focus cycles with a two-dimensional unstable manifold by a chaotic attractor. One can observe the occurrence of a stable limit cycle of period-19 (P^{19} in Fig. 10c) at amplitude A = 1.3. This cycle undergoes a Neimark-Sacker bifurcation as the amplitude decreases, and a stable invariant curve is born in the vicinity of each fixed point in the stroboscopic section. The appearance of two-frequency quasi-periodic oscillations (T^{19} in Fig. 10c) is observed on the graph of Lyapunov exponents; in phase space, such an attractor is represented by 19 invariant curves in the stroboscopic section. The destruction of invariant curves leads to the appearance of

a 19-component chaotic attractor, which is then transformed into a one-component (Fig. 10f). Figure 10g clearly demonstrates that in the structure of the attractor there are areas not filled with points that correspond to the saddle-focus cycle of period-19; this attractor is characterized by only one positive Lyapunov exponent (see Table 4). As parameter A decreases, a homoclinic bifurcation occurs between the saddle-focus cycle of period-19 and the chaotic attractor, as a result the attractor becomes hyperchaotic (see Fig. 10h, Table 4). With a further decrease in the signal amplitude, a homoclinic bifurcation occurs between the base cycle of period-1 and the chaotic attractor, which is also characterized by two positive Lyapunov exponents. We can also observe this scenario with increasing amplitude. At $A = 1.29$ there is a stable limit cycle of period-38 (P^{38} in Fig. 10c). With amplitude increasing cycle P^{38} undergoes Neimark-Sacker bifurcation and 38 invariant curves appear in stroboscopic map (T^{38}). Then it become resonant and hardly transforms to hyperchaos. The hard transition can be associated with mutistability. For Fig.10c we made additional checking: we changed direction of scanning of parameter with continuation of initial conditions, and the hard transition is persist.

Table 4. Values of the Lyapunov exponents for different chaotic attractors observed in non-autonomous model of Anishchenko-Astakhov generator (6) at the threshold of hyperchaos formation, $g = 0.5$, $m = 1.2$

T	A	Λ_1	Λ_2	Λ_3	Λ_4
3.0	1.43	0.0102	0.0	-0.019	-0.8318
3.0	1.296	0.0145	0.0	-0.0081	-0.7835
3.0	1.293	0.0244	0.0092	0.0	-0.8148
3.0	1.21	0.0973	0.0229	0.0	-0.9019

6. Conclusions

We study the dynamics of the model of Anishchenko-Astakhov generator under periodic pulse action. Various cases of choosing the parameters of the autonomous system are considered: periodic and chaotic self-oscillations.

For the case when the autonomous model demonstrates periodic oscillations, it is shown that the synchronization picture is close in structure to the classical synchronization picture observed in a two-dimensional system. However, for a three-dimensional system we reveal the appearance of secondary Neimark-Sacker bifurcations and the development of chaos as a result of the destruction of two-frequency tori. This scenario for the development of chaos leads to the manifestation of the effect of a multi-dimensional system: hyperchaos and chaos with an additional Lyapunov exponent close to zero form. The region in the vicinity of the subharmonic synchronization tongue of period-3, where multi-dimensional chaos appears, is shown on the plane of the "period – amplitude" parameters of the external force. Cascades of bifurcations of invariant torus doubling in this region, as well as cascades of the secondary Neimark-Sacker bifurcations, can be traced. Cascades of bifurcations of invariant torus doubling lead to the formation of a chaotic attractor, in the spectrum of which, in addition to positive and zero, there is Lyapunov exponent close to zero (weakly negative or positive). The absence of a zero exponent can be explained by the finiteness of the bifurcation cascade of tori doublings. Cascades are interrupted by the appearance of resonances, which made impact to dynamics.

For the case when the autonomous dynamics of the model is chaotic, in the non-autonomous case multi-dimensional chaos is also observed. Chaos with an additional Lyapunov exponent close to zero is observed at a small value of external force amplitude. Chaos transforms into classical chaos for large values of the period of external force with increasing amplitude. Chaos with an additional Lyapunov exponent close to zero persists at short periods. There are windows of two-frequency quasi-periodicity within the region with an additional zero Lyapunov exponent. Periodic and quasi-periodic oscillations occur at small periods and signal amplitudes. The transition from periodic oscillations to quasi-periodic can occur as a result of the Neimark-Sacker bifurcation, as well as a result of the saddle-node bifurcation. The development of chaos occurs through doubling of invariant curves with a decrease in amplitude. The development of hyperchaos is observed as a result of the homoclinic bifurcation of the saddle-focus limit cycle and the chaotic attractor in small regions of the parameter plane.

The obtained results open the route to the opportunity of implementation of discrete Shilnikov attractors in the physical experiment. For the best our knowledges nowadays it wasn't shown. The Anishchenko-Astakhov generator is enough simple radio-physical generator, which can be realized with analog electronic base. Kicked by pulses generator would be allow to demonstrate discrete Shilnikov attractors in the experiment. We plan to continue our work in this direction. Another work for future is tried to obtain multi-dimensional chaos in the model with another way of complification. Instead external force it can be considered the effects of fractional order [50-53].

Acknowledgments

The study of autonomous periodic self-oscillated case was supported by the Ministry Of Science and Higher Education of the Russian Federation, agreement no. 075-15-20220287 (Sections 1, 3, 4.1, 4.2, 6). The study of the van der Pol oscillator (Section 2) and case of autonomous chaotic self-oscillations (Section 5) was prepared by AK, NS as the investigation (No. 23-00-028) in the frame of program "Scientific Foundation of HSE University" in 2023-2024. Investigation of Shilnikov discrete attractors (Section 4.3) were preformed by NS with financial support of Russian Science Foundation (project 20-71-10048, https://rscf.ru/project/23-71-50011/).

Data Availability

Data supporting numerical experiments presented in this paper are available from the corresponding author upon reasonable request.

Declaration of generative AI and AI-assisted technologies in the writing process

During the preparation of this work the authors used **DeepL Write** in order to improve language. After using this tool, the authors reviewed and edited the content as needed and take full responsibility for the content of the publication.

Declaration of Competing Interest

Authors declare that they have no conflict of interest.

Author contributions

N.S. conceptualized the study. A.K. performed the numerical simulations and bifurcation analysis with help of P.P. and N.S. N.S. and A.K. interpreted the results and wrote the manuscript.

Reference

[1] Pikovsky A., Rosenblum M., Kurths J. Synchronization: a universal concept in nonlinear science, Cambridge University Press. 2001.

[2] Balanov A., Janson N., Postnov D., Sosnovtseva O. Synchronization: From simple to complex. Springer. 2009.

[3] Shilnikov A., Shilnikov L., Turaev D. On some mathematical topics in classical synchronization: A tutorial. International Journal of Bifurcation and Chaos 2004; 14(07): 2143-2160.

[4] Glass L., Sun J. Periodic forcing of a limit-cycle oscillator: Fixed points, Arnold tongues, and the global organization of bifurcations. Physical Review E 1994; 50(6): 5077.

[5] Mosekilde E., Maistrenko Y., Postnov D. Chaotic synchronization: applications to living systems. World Scientific. 2002.

[6] Gonzalez-Miranda J. M., Synchronization and control of chaos: an introduction for scientists and engineers. World Scientific. 2004.

[7] Kuznetsov S.P., Sataev I.R. Universality and scaling for the breakup of phase synchronization at the onset of chaos in a periodically driven Rössler oscillator. Physical Review E 2001; 64(4): 046214.

[8] Kuznetsov A.P., Stankevich N.V., Tyuryukina L.V. Features of pulsed synchronization of an autooscillatory system with a three-dimensional phase space. Technical physics letters 2006; 32(4); 343-346.

[9] Kuznetsov A.P., Stankevich N.V., Turukina, L. V. Stabilization by external pulses and synchronous response in the Rössler system before saddle-node bifurcation. Russian Journal of Nonlinear Dynamics 2009; 5(2): 253-264. (in Russia)
[10] Shulgin B., Stone L., Agur Z. Pulse vaccination strategy in the SIR epidemic model, Bulletin of mathematical biology 1998; 60: 1123 – 1148.
[11] Li Q., Xiao Y. Dynamical behavior and bifurcation analysis of the SIR model with continuous treatment and state dependent impulsive control. International Journal of Bifurcation and Chaos 2019; 29: 1950131.
[12] Wang L., Existence of periodic solutions of seasonally forced SEIR models with pulse vaccination. Discrete Dynamics in Nature and Society 2020; 9381375.
[13] Etxeberria-Etxaniz M., Alonso-Quesada S., De la Sen M. On an SEIR epidemic model with vaccination of newborns and periodic impulsive vaccination with eventual on-line adapted vaccination strategies to the varying levels of the susceptible subpopulation. Applied Sciences 2020; 10: 8296.
[14] Berhe H.W., Al-arydah M. Computational modeling of human papillomavirus with impulsive vaccination. Nonlinear Dynamics 2021; 103: 925–946.
[15] Tang B., Li Q., Xiao Y., Sivaloganathan S. A novel hybrid model of tumor control, combining pulse surveillance with tumor size-guided therapies. Applied Mathematical Modelling 2022; 104: 259-278.
[16] Piotrowska M.J., Puchalska A., Sakowski K. On the network suppression of the pathogen spread within the healthcare system. Applied Mathematics and Computation 2023; 457: 128169.
[17] Klinshov V., Shchapin D., Yanchuk S., Nekorkin V. Jittering waves in rings of pulse oscillators. Phys. Rev. E 2016; 94: 012206.
[18] Klinshov V., Nekorkin V. Event-based simulation of networks with pulse delayed coupling. Chaos 2017; 27: 101105.
[19] Klinshov V. V., D'Huys O. Noise-induced switching in an oscillator with pulse delayed feedback: A discrete stochastic modeling approach. Chaos 2022; 32: 093141.
[20] Blokhina E., Feely O. A kicked oscillator as a model of a pulsed MEMS system. International Journal of Bifurcation and Chaos 2009; 19: 187-202.
[21] Vubangsi M., Tchoffo M., Fai L.C. Quantum dynamics of a kicked system with position-dependent effective mass. The European Physical Journal Plus 2014; 129: 1-7.
[22] David G., Esat K., Hartweg S., Cremer J., Chasovskikh E., Signorell R. Stability of aerosol droplets in Bessel beam optical traps under constant and pulsed external forces. J. Chem. Phys. 2015; 142: 154506.
[23] Stankevich N.V. Stabilization and complex dynamics initiated by pulsed force in the Rössler system near saddle-node bifurcation. Nonlinear Dynamics. 2024; 112(4): 2949-2967.
[24] Liu G., Cui C., Wang K., Han B., Zheng S. Sensorless control for high-speed brushless DC motor based on the line-to-line back EMF. IEEE Transactions on Power Electronics. 2014; 31(7): 4669-4683.
[25] Zhang H., Wu H., Jin H., Li H. High-dynamic and low-cost sensorless control method of high-speed brushless DC motor. IEEE Transactions on Industrial Informatics. 2022; 19(4): 5576-5584.
[26] Kanamaru T. Van der Pol oscillator. Scholarpedia 2007; 2(1): 2202.
[27] Kuznetsov A.P., Seliverstova E.S., Trubetskov D.I., Turukina L.V. Phenomenon of the van der Pol equation. Izvestiya Vuzov. Applied nonlinear dynamics 2014; 22(4): 3-42. (in Russia).
[28] Sprott J.C. A proposed standard for the publication of new chaotic systems. International Journal of Bifurcation and Chaos 2011; 21(09): 2391-2394.
[29] Benettin G., Galgani L., Giorgilli A., Strelcyn J.M. Lyapunov characteristic exponents for smooth dynamical systems and for Hamiltonian systems; a method for computing all of them. Part 1: Theory. Meccanica 1980; 15: 9-20.
[30] Kuznetsov N.V. The Lyapunov dimension and its estima tion via the Leonov method. Phys. Lett. A. 2016; 380: 2142–2149.

[31] Kuznetsov N.V., Leonov G.A., Mokaev T.N., Prasad A., Shrimali M.D. Finite-time Lyapunov dimension and hidden attractor of the Rabinovich system. Nonlinear Dynamics. 2018; 92: 267–285.
[32] Holmes P. J., Rand D. A. Bifurcations of the forced van der Pol oscillator. Quarterly of Applied Mathematics 1978; 35(4): 495-509.
[33] Kuznetsov A.P., Turukina L.V. Van der Pol oscillator with pulse action: from differential equation to map. Izvestiya Vuzov. Applied nonlinear dynamics 2001; 9(6): 69-82. (in Russia).
[34] Anishchenko V.S. Dynamical chaos: models and experiments: appearance routes and structure of chaos in simple dynamical systems, World Scientific. 1995.
[35] Ermentrout B.G. Simulating, Analyzing, and Animating Dynamical Systems: A Guide to XPPAUT for Researchers and Students. SIAM, Philadelphia. 2002.
[36] Stankevich N.V., Dvorak A., Astakhov V., Jaros P., Kapitaniak M., Perlikowski P., Kapitaniak T. Chaos and hyperchaos in coupled antiphase driven Toda oscillators. Regular and Chaotic Dynamics 2018; 23: 120-126.
[37] Stankevich N., Kuznetsov A., Popova E., Seleznev E. Chaos and hyperchaos via secondary Neimark–Sacker bifurcation in a model of radiophysical generator. Nonlinear dynamics 2019; 97(4): 2355-2370.
[38] Garashchuk I.R., Sinelshchikov D.I., Kazakov A. O., Kudryashov N.A. Hyperchaos and multistability in the model of two interacting microbubble contrast agents. Chaos 2019; 29(6): 063131.
[39] Sataev I.R., Stankevich N.V. Cascade of torus birth bifurcations and inverse cascade of Shilnikov attractors merging at the threshold of hyperchaos. Chaos 2021; 31(2): 023140.
[40] Shykhmamedov A., Karatetskaia E., Kazakov A., Stankevich N. Scenarios for the creation of hyperchaotic attractors in 3D maps. Nonlinearity 2023; 36(7): 3501.
[41] Stankevich N.V., Shchegoleva N.A., Sataev I.R., Kuznetsov A.P. Three-dimensional torus breakdown and chaos with two zero Lyapunov exponents in coupled radio-physical generators. Journal of Computational and Nonlinear Dynamics 2020; 15(11): 111001.
[42] Kuznetsov A.P., Sedova Y.V., Stankevich N.V. Coupled systems with quasi-periodic and chaotic dynamics. Chaos, Solitons & Fractals 2023; 169: 113278.
[43] Broer H.W., Vitolo R., Simó C. Quasi-periodic Hénon-like attractors in the Lorenz-84 climate model with seasonal forcing. In EQUADIFF 2003 2005: 601-606.
[44] Broer H.W., Simó C., Vitolo R. Quasi-periodic Hénon-like attractors in 3D diffeomorphisms. ENOC-2005 2005: 7-12.
[45] Shena J., Lazarides N., Hizanidis J. Multi-branched resonances, chaos through quasiperiodicity, and asymmetric states in a superconducting dimer. Chaos 2020; 30(12): 123127.
[46] Broer H.W., Huitema G.B., Takens F., Braaksma B.L.J. Unfoldings and Bifurcations of Quasi-periodic Tori. Amer. Matj. Soc. 1990.
[47] Vitolo R., Broer H., Simó C. Quasi-periodic bifurcations of invariant circles in low-dimensional dissipative dynamical systems. Regular and chaotic dynamics 2011; 16: 154-184.
[48] Stankevich N.V., Kuznetsov A.P., Seleznev E.P. Chaos and hyperchaos arising from the destruction of multifrequency tori. Chaos, Solitons & Fractals 2021; 147: 110998.
[49] Sekikawa M., Inaba N. Chaos after accumulation of torus doublings. International Journal of Bifurcation and Chaos 2021; 31(01): 2150009.
[50] Guo B., Pu X., Huang F. Fractional partial differential equations and their numerical solutions. World Scientific. 2015.
[51] Sheu L.J., Chen H.K., Chen J.H., Tam L.M. Chaotic dynamics of the fractionally damped Duffing equation. Chaos, Solitons & Fractals. 2007; 32(4): 1459-1468.
[52] Kai Y., Chen S., Zhang K., Yin Z. Exact solutions and dynamic properties of a nonlinear fourth-order time-fractional partial differential equation. Waves in Random and Complex Media. 2022: 1-12.

[53] Wang R., Feng Q., Ji J. The discrete convolution for fractional cosine-sine series and its application in convolution equations. AIMS Mathematics. 2024; 9(2): 2641-2656.